Deformable stochastic boundaries in molecular dynamics[a)]

C. L. Brooks III and M. Karplus
Department of Chemistry, Harvard University, Cambridge, Massachusetts 02138

(Received 28 June 1983; accepted 31 August 1983)

A new approach to studying localized chemical events in condensed phases is developed. The approach provides a simple and convenient method for reducing the total number of solvent particles explicitly included in simulations of localized processes while decreasing spurious edge effects. Both energy flow across the boundary and density fluctuations in the simulation region are included; this makes it possible to treat nonequilibrium processes, such as thermal gradients and endothermic or exothermic chemical reactions. The essential element of the approach is the introduction of a soft boundary force and a stochastic buffer region. For simple liquids, the boundary force is determined from the solvent equilibrium structure (radial distribution function) and is readily incorporated into conventional molecular dynamics algorithms. The methodology is illustrated by application to liquid argon in spherical and cubical simulation regions; comparison with standard molecular dynamics results show excellent agreement for structural, dynamic, and thermodynamic properties.

I. INTRODUCTION

Molecular dynamics and Monte Carlo simulations have contributed in recent years to revolutionizing our understanding of condensed phases.[1] A wealth of structural, thermodynamic, and dynamic information has become available and in combination with developments in the statistical mechanical theory of liquids[2] and in experimental techniques (e.g., neutron scattering and picosecond spectroscopy) has brought this once difficult and esoteric area to the center of present day physical chemistry. Based on a knowledge about pure fluids and fluid mixtures at equilibrium, attempts are now being made to extend simulation techniques to nonequilibrium phenomena, including chemical reactions in solutions,[3–5] and to amorphous systems like the interior of proteins.[6] Such extensions introduce a number of problems that require methodological developments.

Any dynamical simulation requires that the true macroscopic system composed of on the order of 10^{23} particles be replaced by a microscopic sample of only 10^2 to 10^4 particles. The "method of choice" for such a reduction is the introduction of periodic boundary conditions with the central cell, whose dynamics is being considered explicitly, surrounded by image cells.[7] In this way a small sample can be treated while minimizing edge effects; that edge effects are not eliminated completely has been pointed out and approaches to correcting them have been suggested.[8] When one focuses on inhomogeneous systems and nonequilibrium phenomena, a number of difficulties arise with the straightforward application of periodic boundary conditions. An example of a nonequilibrium system is one where a thermal gradient is present and destroys the possibility of a periodic boundary treatment. For simulations involving chemical reactions that can act as sources or sinks of energy and introduce density gradients, corresponding problems arise. Chemical reactions raise the additional difficulty that they are often slow on a simulation time scale (e.g., due to the presence of energy barriers) and that a straightforward molecular dynamics simulation would not be feasible.

Systems that are inhomogenous even though at equilibrium include amorphous solids, clusters, proteins, and interfaces. For none of these is there a simple periodic set of cells that can be used to provide an adequate representation. In the case of interfaces, simulations with periodic boundary condition have, in fact, been done though the model systems are somewhat artificial.[9] Alternatively, it is sometimes possible to take a system that is sufficiently large that the boundary plays a relatively minor role. A case in point is provided by recent protein simulations,[6] where isolated molecules have been studied with the assumption that the atoms in the interior will be shielded by the surrounding protein atoms from effects due to the absence of a solvent environment. Of course, for certain problems (e.g., water clusters), the physical system consists of a small number of interacting molecules isolated in vacuum,[10] so that the edge effects in the calculation would be present in reality.

To circumvent the difficulties with standard periodic boundary simulations, a number of approaches have been proposed, the nature of the method depending somewhat on the problem being examined. One type uses molecular dynamics but confines the system to a finite volume and thereby avoids the need for periodicity. The treatment of the system boundary then plays an important role and several approaches have been tried; they include the use of rigid walls for a gas-phase recombination reaction[3] or a protein side chain isomerization reaction,[11] thermalized walls for treating heat conduction in a thermal gradient[12] and walls that move with the central atom of the system being simulated.[13] To extend the effective time range of simulations, whether in a periodic or finite volume system, activated dynamics methods have been adapted from gas-phase molecular collision studies[14,15] to solution conditions.[16] Finally, explicit treatment of the solvent has been avoided for cases where only a single molecule or a small number are of primary interest by the introduction of stochastic dynamics[17]

[a)] Supported in part by a grant from the National Science Foundation.

 0021-9606/83/246312-14$02.10

based on the simple or generalized Langevin equation.[18]

Although applications of the approaches described above have led to considerable progress in our knowledge of chemical events in condensed phases, further development of the methodology is required. Of particular importance is the availability of a general method that makes it possible to treat explicitly by molecular or activated dynamics techniques relatively small numbers of particles in a nonperiodic system, yet avoids effects introduced by imposing a rigid or simple stochastic boundary. Specifically, it is necessary to eliminate effects of the boundary on the primary region under consideration; that is, the solution of the dynamical equations should yield a correct description of the particle motions, energy flow across the boundary should be possible and density variations within the reaction volume should be able to occur. The essential problem in developing such an approach for a finite system is to take account of the effects of the particles outside the region of interest without specifically accounting for their dynamics. The present paper, which is an extension of earlier studies already mentioned,[3,12,13] introduces a method for so doing without violating the requirements for a satisfactory boundary. The system to be studied is divided into three regions; an inner (reaction) region in which the particles are treated explicitly by molecular dynamics, a surrounding buffer region, in which the particles are treated explicitly by stochastic dynamics, and a deformable boundary, whose forces on the particles in the reaction and buffer region arise from the average structure of the system beyond the boundary. The approach is directly applicable to dilute solution reaction dynamics, as well as to the solvent boundary at the active site of a protein; alternative techniques for treating boundaries in the protein interior are being developed. It is possible also to use the method for cases that are finite and nonhomogeneous in one dimension, but for which periodic boundary conditions would be appropriate in the other dimensions; an example is the simulation of a system in a thermal gradient.

In Sec. II, we briefly review previous approaches to simulating boundary effects. This motivates our development of the deformable boundary force and the deformable stochastic boundary method described in Sec. III. The method proposed accounts for localized energy and density fluctuations. We use the well-studied case of Lennard-Jones argon particles to illustrate the method. The results are presented in Sec. IV. We first determine the form of the forces arising from the deformable boundary and compare it with the rigid boundary results of Stace and Murrell.[3] We then present several molecular dynamics simulations that use the deformable stochastic boundary approach and compare these test cases with conventional molecular dynamic results.[1] Section V includes a summary discussion of the method and its possible applications and extensions. In the Appendix, we give simulation results for the Lennard-Jones–Devonshire model[3,19] for comparison with the present treatment.

II. PRIOR TREATMENTS OF FINITE SYSTEMS

Several methods have been proposed for the simulation of finite representatives of infinite systems in the absence of periodic boundary conditions. We briefly review these approaches here, since some of the ideas on which they are based provide motivations for the present treatment.

Stace and Murrell[3] studied the recombination of radical atoms in a gas by treating a system composed of only eight atoms confined to a spherical box. The force exerted by the wall of the box on the simulation particles was derived from an idea developed by Lennard-Jones and Devonshire in their cell theory for liquids.[19] A uniform spherical shell of thickness σ consisting of Lennard-Jones particles with their center located at the boundary surface of the simulation box was introduced. As a result of the spherical symmetry, the force acting on each particle due to this wall is radially directed. No energy exchange with the surroundings is included. Reasonable qualitative results for the recombination dynamics were obtained with the model, although no analysis was made of the effects of this simple "wall force" on local properties; a simulation study employing this model is included in the Appendix.

Ciccotti, Tenenbaum, and Gallico[12] have recently developed a method for studying the dynamics of particles in thermal gradients in the presence of a hard stochastic (thermal) wall that yields a canonical ensemble.[20] In this approach, a particle which crosses a simulation boundary reenters the system by reflection off a wall with a random thermal velocity, $\mathbf{v}$, chosen such that $\mathbf{e}_n \cdot \mathbf{v} > 0$, where $\mathbf{e}_n$ is an inward pointing normal to the boundary. No interactions with particles outside the wall are included. In the actual simulation, such a hard stochastic wall was used in only one spatial direction, periodic boundary conditions being employed in the other two. The method allows one to study equilibrium processes as well as dynamics in steady-state thermal gradients. It suffers from the possibility of spurious edge effects due to the absence of more realistic boundary forces; it was argued that edge effects were unimportant in the simulations reported.[12]

Closest in spirit to the present approach is a method recently proposed by Berkowitz and McCammon.[13] These authors decomposed the many-body system into two major spherical regions, a static reservoir region and a reaction zone and further divided the reaction zone into a reaction region and a buffer region. The static reservior region surrounds the reaction zone and serves to diminish spurious edge effects. The configuration of the particles within the reservior region is fixed so as to limit the dynamics to the reaction zone; a particular configuration of particles is chosen from a prior molecular dynamics or Monte Carlo simulation of a much larger system. The buffer region between the reservior and reaction regions is composed of particles whose dynamics are determined by a simple Langevin equation; this provides a thermal sink/source for the particles in the reaction region which obey a molecular dynamics algorithm. All particles in the reaction and buffer region interact with each other and with the particles in the reservior region, subject to an appropriate cut off radius. The entire system (reservior, buffer, and reaction regions) moves with the central particle under consideration through a much larger simulation box. In an application to liquid argon with the three regions consisting of 86, 26, and 179 particles, respectively, the authors obtained a radial distribution function relative to the central particle and a velocity autocorrelation function

for the central particle in reasonable agreement with the results of a standard dynamical simulation.

Although the approach of Berkowitz and McCammon[13] provides many of the essentials for simulating localized chemical events, the treatment of the effects of the surrounding atoms requires additional consideration. Since a particular particle configuration is used for representing the reservoir region, the dynamics within the reaction region may be biased. Further, the reservoir region is rather extensive and all force centers composing it must be included for the dynamics of the particles within the reaction zone; e.g., in the case considered, there were only 112 particles in the reaction zone and 179 static particles in the reservoir region. Finally, since the entire system moves with the central particle, a large volume of particle positions, in addition to those in the reservoir region, must be available.

III. METHOD

In this section, we develop the present approach. We first introduce the nature of the deformable boundary and its consequences and then describe the buffer zone that provides for energy flow in and out of the system.

A. Deformable boundaries: The mean field force approximation

The present approach to simulating the effects of the boundary region surrounding a simulation zone is based on the ideas developed by Stace and Murrell[3] and by Berkowitz and McCammon.[13] The entire system of interest is partitioned into a boundary region and a simulation zone. The simulation zone is treated in a manner similar to that employed by Berkowitz and McCammon; that is, it is divided into a reaction region, the particles of which are treated by molecular dynamics, and a stochastic buffer region. An essential new element of the present approach is in the treatment of the boundary region. Rather than introducing a particular configuration of particles in a reservior region, we assume that forces on particles within the simulation zone due to particles beyond the boundary arise from the average structure. For simple liquids, therefore, only a knowledge of the pair (radial) distribution function is required. The dynamical simulation of the simulation zone is then carried out by conventional techniques with the addition of a "deformable boundary force" arising from mean field interactions with particles beyond the boundary. In the simplest cases, this additional mean field force depends only on the distance of the simulation particles from the boundary. Furthermore, as in the treatment of Ciccotti *et al.*,[12] such a boundary force can be used in conjunction with periodic boundaries at surfaces where they are appropriate. The equations for the mean field force approximation (MFFA) boundaries are now developed for several specific examples to illustrate the approach.

1. 2D circular boundary

It is instructive to consider first the two-dimensional problem of N identical disks enclosed by a circular boundary of radius R. The disks are in a thermodynamic state described by a temperature T; mean surface density

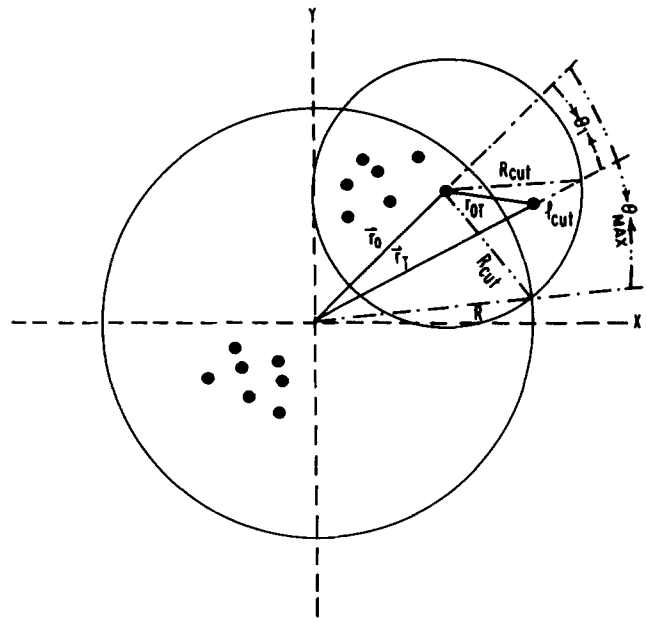

FIG. 1. Conceptual picture and geometric details for the 2*D* deformable boundary force calculation. The particle of interest (particle zero) is located at $\mathbf{r}_0$ within the simulation box of radius 12.0 Å. The "test particle," which is located at $\mathbf{r}_T$ outside the circle of radius R but inside the cutoff circle of radius R_{cut}, exerts an effective force on particle zero. This force [Eq. (3)] is given by the LJ force arising from the interaction at separation r_{0T} multiplied by the probability of the test particle being there, which is related to $g(r_{0T})$. The integration limits, including l_{cut} and θ_{max}, are dictated by the geometrical considerations illustrated here.

$\rho = N/\pi R^2$, where R is the radius of the simulation circle; and a pair distribution $g(r)$, where $r = |\mathbf{r}_i - \mathbf{r}_j|$. It is assumed that the particles interact via a pairwise additive potential $u(r)$ and that the potential is cut off at some characteristic range, R_{cut}. A truncated potential is not necessary but it will be used here for simplicity; switching functions can be employed.

The system is illustrated in Fig. 1. We wish to determine the total force on the particle labeled zero at $\mathbf{r}_0 = (x_0, y_0)$ due to all of the particles (real and virtual) within the circle of radius R_{cut}. The contribution from particles within the simulation zone at a distance less than R_{cut} is just the usual sum over pair interactions employed in molecular dynamics. The contribution due to the virtual particles within the distance R_{cut} but outside of the simulation zone may be obtained by placing a test particle at $\mathbf{r}_T$; calculating the force on particle zero due to the test particle, weighted by the probability of a particle being a distance r_{0T} from particle zero, $\rho g(r_{0T})$; and summing the forces resulting from all possible positions of the test particle. We note that configurational many-body effects due to the other $N-1$ particles within the simulation zone are tacitly ignored in assuming that the probability of finding a particle at a distance r_{0T} from particle zero is given by $\rho g(r_{0T})$. With this procedure, the boundary force from the virtual particles acting on particle zero is given by (see Fig. 1):

$$F_W(r_0) = 2\int_0^{\theta_{max}} d\theta_T \int_R^{l_{cut}(\theta_T)} dr_T\, r_T\, F(\mathbf{r}_{0T})\rho g(r_{0T}) \qquad (1)$$

with $\theta_{\max}$ determined from $r_0 = |\mathbf{r}_0|$, R, and R_{cut} as

$$\theta_{\max} = \cos^{-1}\left[\frac{(R^2 + r_0^2 - R_{\text{cut}}^2}{2Rr_0}\right]$$

and the distance l_{cut} given by

$$l_{\text{cut}}(\theta_T) = r_0 \cos\theta_T + \sqrt{(r_0\cos\theta_T)^2 + R_{\text{cut}}^2 - r_0^2}.$$

The quantity $F(\mathbf{r}_{0T})$ is the component of the force along the direction $\hat{\mathbf{r}}_0$ where $\hat{\mathbf{r}}_0 = \mathbf{r}_0/r_0$ arising from the potential $u(r_{0T})$; that is,

$$F(\mathbf{r}_{0T}) = \left(\frac{r_T\cos\theta_T - \mathrm{r}_0}{r_{0T}}\right)\frac{\partial u(r_{0T})}{\partial r_{0T}}.$$

Only this component is required since, due to the symmetry with respect to $\mathbf{r}_0(\theta_T = 0)$ the boundary force, $F_W(r_0)$, is radial and directed along $\hat{\mathbf{r}}_0$; we write the radial component as $F_W(r_0)$. Thus, the boundary force can be decomposed into its x and y components in the dynamics reference frame (Fig. 1) by

$$\mathbf{F}_B(\mathbf{r}_0) = \hat{\mathbf{r}}_0 F_W(r_0). \tag{2}$$

2. 3D spherical boundary

The extension of the boundary force calculation from a $2D$ circular boundary to a $3D$ spherical boundary follows from the fact that there is azimuthal symmetry in the $3D$ problem. One can write immediately that the $3D$ radial boundary force is

$$F_W(r_0) = 4\pi\int_{x_{\max}}^{1} dx_T \int_R^{l_{\text{cut}}(x_T)} dr_T\, r_T^2\, F(\mathbf{r}_{0T})\rho g(r_{0T}), \tag{3}$$

with $x_T = \cos\theta_T$ and $\mathbf{F}_B(\mathbf{r}_0) = \hat{\mathbf{r}}_0 F_W(r_0)$.

3. Combination boundaries: Deformable and periodic

In some cases it is convenient to use a simulation box which is a cube or parallelopiped and has periodic boundaries along some directions and a deformable boundary force along others. Examples include the thermal gradient studied by Ciccotti *et al.*,[12] and solvent dynamics around an exposed active site of a protein or at a liquid–solid interface (see Sec. V). A system with periodic boundaries in the x and z directions and a deformable boundary force directed along the y axis is illustrated in Fig. 2. For the $2D$ case, the boundary force acting on a particle with y coordinate, y_0, is in the y direction and has the form,

$$F_W(y_0) = 2\int_0^{\theta_{\max}} d\theta_T \int_{l_{\min}(\theta_T)}^{l_{\max}(\theta_T)} dr_T\, r_T F(\mathbf{r}_{0T}) \times \rho g(r_{0T});\ \mathbf{F}_B(y_0) = \begin{bmatrix} 0 \\ F_W(y_0) \end{bmatrix}. \tag{4a}$$

In the $3D$ case, we have the corresponding expression

$$F_W(y_0) = 4\pi\int_{x_{\max}}^{1} dx_T \int_{l_{\min}(x_T)}^{l_{\max}(x_T)} dr_T\, r_T^2 F(\mathbf{r}_{0T}) \times \rho g(r_{0T});\ \mathbf{F}_B(y_0) = \begin{bmatrix} 0 \\ F_W(y_0) \\ 0 \end{bmatrix}. \tag{4b}$$

Here

$$\theta_{\max} = \tan^{-1}\left[\frac{(R_{\text{cut}}^2 - (L/2 - y_0)^2)^{1/2}}{L/2}\right]$$

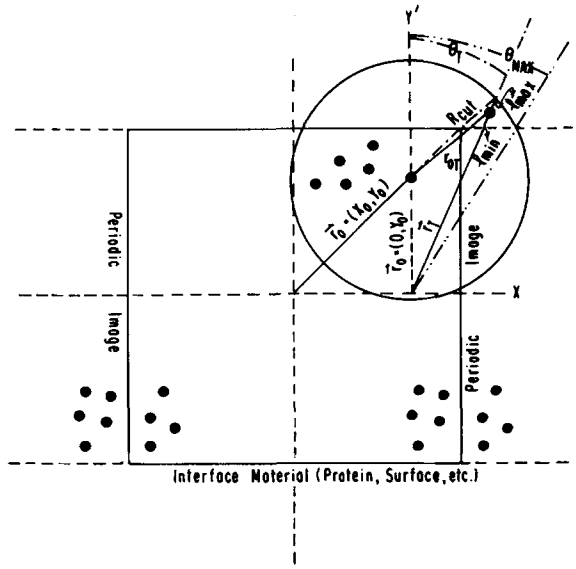

FIG. 2. Conceptual picture and geometrical details for the deformable boundary force for the case of particles within a semi-infinite (in two dimensions) cubic simulation box. In this figure only the X and Y directions are displayed; the Z direction is treated the same as the X direction (with periodic boundaries). The information contained in the illustration is similar to that of Fig. 1; This specific simulation set-up could be used to include solvent along the surface of a protein or at a liquid/solid interface by replacing the deformable boundary on the $-Y$ axis with the material of interest.

and

$$l_{\min}(x_T) = (L/2)/x_T;$$

$$l_{\max}(x_T) = (y_0 x_T) + \sqrt{(y_0 x_T)^2 + R_{\text{cut}}^2 - y_0^2}.$$

The examples given here demonstrate that the deformable mean field boundary force is straight forward to calculate for realistic simulation systems. It provides a simple method for including average many-body effects in simulations of restricted volumes around a simulation zone. For the cases considered here, the boundary force has several additional computationally convenient and theoretically desirable properties. The boundary force is a function only of the separation of the particle from the boundary. Thus, it can be tabulated in a one-dimensional array and is easily incorporated into conventional molecular dynamics algorithms. For simulation zones of sufficient size the boundary force decreases to zero as r_0 approaches zero so that particles near the center of the simulation region do not feel its effects. Because the boundary force depends on the mean configuration of the surrounding virtual particles, the net average force on a particle within the simulation box vanishes as it should; this condition is not necessarily met by the method proposed by Berkowitz and McCammon.[13] Finally, the nature of the boundary force is such that density fluctuations can occur.

B. Fluctuating stochastic boundaries

Although the deformable mean field boundary makes possible realistic simulations without periodic boundary conditions, thermal relaxation is not included. Both Ciccotti *et al.*[12] and Berkowitz and McCammon[13] have utilized sto-

chastic techniques to simulate thermal relaxation in a localized region of a many-body system. Here we propose a method for incorporating thermal fluctuations analogous to that of Berkowitz and McCammon,[13] in the framework of the mean field deformable boundary approximation. In this way, we are able to include thermal and density relaxations simultaneously; this is expected to be of particular importance for exothermic or endothermic reaction systems.

The simulation zone introduced above is now divided into two parts. There is an inner reaction region, in which particles propagate according to molecular dynamics with the addition of any boundary forces that contribute and an outer buffer region, in which particles propagate according to the Langevin equation, again with the addition of the boundary forces.

For the system with a deformable boundary and a stochastic buffer region, the forces on a particle at $\mathbf{r}_0$, in addition to the systematic force due to explicit two-particle interactions, depend on the region in which the particle is located. There are three regions: the inner reaction region ($r_0 \leqslant R_B$), the stochastic buffer region ($R_B < r_0 \leqslant R$), and the boundary region ($r_0 \geqslant R$). Considering a spherical system, we can write the additional force, $\mathbf{F}_B(\mathbf{r}_0)$, in each of these regions as

$$\mathbf{F}_B(\mathbf{r}_0) = \begin{cases} \hat{\mathbf{r}}_0 F_W(r_0), & r_0 \leqslant R_B, \\ \hat{\mathbf{r}}_0 F_W(r_0) - \beta \mathbf{v} + \mathbf{f}(t), & R_B < r_0 \leqslant R, \\ \hat{\mathbf{r}}_0 F_W^L(r_0) - \beta \mathbf{v} + \mathbf{f}(t), & r_0 \geqslant R. \end{cases} \tag{5}$$

For the reaction region ($r_0 \leqslant R_B$), the only additional force is that due to the boundary; the expression is identical to Eq. (3). For the buffer region, there is a corresponding boundary force augmented by terms that are associated with conventional Langevin dynamics; i.e., a dissipative force $-\beta \mathbf{v}(t)$, and a random force $\mathbf{f}(t)$. The friction coefficient, β, is related to the bulk diffusion constant via the Einstein relationship, and the random force is the usual Gaussian white noise source with properties $\langle \mathbf{f}(t) \rangle = 0$ and

$$\langle \mathbf{f}(t) \cdot \mathbf{f}(0) \rangle = 6 k_B T \beta \delta(t).$$

Finally, there is included that possibility that particles will be in the boundary region itself ($r_0 \geqslant R$). It is such particles which give rise to variations of the density in the reaction zone. To treat them appropriately, it is necessary to extend the boundary force in such a way that it remains repulsive. We use a simple linear fit to F_W at $r_0 \cong R$, called F_W^L, to represent the force in this region; numerical details are given in Sec. IV. Other than the replacement of F_W by F_W^L, the boundary particles are treated in the same way by use of a Langevin equation as are the particles in the buffer region. It is clear from Eq. (5) that simulations employing only a deformable boundary force may be carried out by setting $\beta = 0$; the stochastic buffer region is included when β is nonzero.

The forces and boundary conditions given in Eq. (5) permit local density fluctuations in the simulation region due to the "soft" nature of the boundary force. Furthermore, the algorithm maintains thermal equilibrium or permits the system to approach equilibrium for the case of thermal relaxation.

IV. RESULTS

In this section, the deformable mean field boundary force is determined for a number of cases and simulation results making use of the boundary force are presented.

A. Mean field boundary force

Results for the boundary forces calculated for test cases representing a $3D$ sphere of 12 Å radius and 19.4 Å cube are described. As a model system we consider Lennard-Jones argon particles ($\sigma = 3.4$ Å, $\epsilon/k_B = 120$ K) at a temperature $T = 97$ K with mean number density $\rho_0 = 0.020\,54$ Å^{-3}; a cutoff (R_{cut}) for the interaction potential of 2.25σ is used.[21(a)] A suitable criterion for choosing the size of the simulation box is that the "reaction site" be surrounded by one shell of solvent particles which are initially at least a distance R_{cut} from the boundary. In the cases considered here the reaction site is centered at the origin with a radius of $\sigma/2$ since the "reaction" is the dynamics of a single particle; this implies that $R = \sigma + R_{\text{cut}}$. Thus, the 12 Å sphere meets the size criterion but the cubic box does not; the dimensions of the cube were chosen in the present tests to obtain a volume equal to that of the sphere.

Evaluation of the boundary force as defined in Eqs. (3) and (4b) for a sphere and cube, respectively, requires knowledge of the bulk radial distribution function. This could have been obtained from the literature, but for the sake of consistency, it was computed from a conventional molecular dynamics simulation (see Sec. IV B). The numerical calculation of the double integrals appearing in Eqs. (3) and (4b) is accomplished by means of an extended trapezoidal rule generalized to integrals of more than one dimension.[22] The convergence of the resulting integral was verified by increasing the number of grid points used and also by comparing the integrals at selected values of r_0 with those obtained from an integration scheme of higher accuracy.[23]

The deformable MFFA boundary forces due to a spherical boundary of a 12.0 Å sphere and plane boundaries at $z = \pm 9.67$ Å of a 19.34 Å cube are shown in Figs. 3(c) and 3(d); in both cases the force depends only on a single distance parameter as is indicated in the figures. The boundary forces display the anticipated behavior. Particles near the center of the simulation box feel no direct effect from the boundary force; as the particles move toward the boundary they first experience an attractive force and then a strong repulsion.

To understand the detailed behavior of the MFFA boundary forces, it is instructive to consider the spherical case and compare the force with that arising from a single Lennard-Jones particle fixed at $R = 12.0$ Å and with the boundary force arising from a uniform distribution of Lennard-Jones particles on the surface of a 12 Å sphere (i.e., Lennard-Jones Devonshire cell model)[3,19]; these results are shown in Figs. 3(a) and 3(b), respectively.

The forces in Figs. 3(a) and 3(b) are very similar to each other. A particle moving toward the boundary first experiences a net attractive force and then begins to feel the repulsive force due to interaction with the nearest particle or particles on the surface. The repulsive forces are very large near the surface of the sphere and go to $-\infty$ (see the Appendix) due to the rigid nature of the surface. As expected, the attrac-

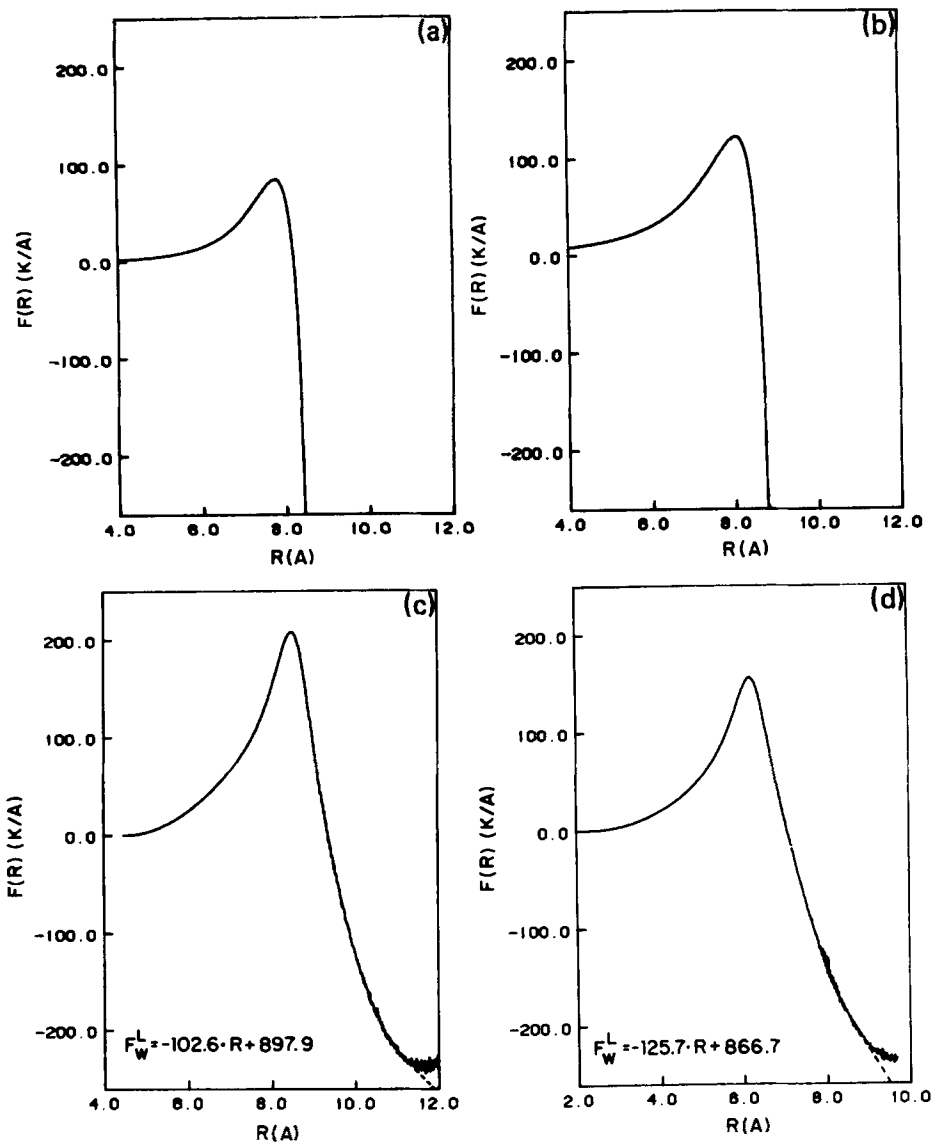

FIG. 3. Boundary force models. The boundary force (in units of K/Å) on an internal particle is plotted vs the separation of the particle from the origin for: (a) a single LJ boundary particle located at $R = 12.0$ Å; (b) a uniform shell of LJ boundary particles located on the surface of a 12.0 Å radius sphere; (c) a deformable boundary located at the surface of a 12.0 Å radius sphere [see Eq. (3)]; (d) a deformable boundary located at one face of a 19.4 Å cube. [The plane boundary is located at a distance of 9.67 Å from the origin along a given axis (see Eq. 4(b) and the discussion of Sec. III).] The inserts in (c) and (d) give the linearized form of the boundary force.

tive peak due to the Lennard-Jones particle surface is slightly larger than that from a single particle.

Comparing the MFFA model [Figs. 3(c) and 3(d)] with the results in Figs. 3(a) and 3(b), we see that the force curves show corresponding behavior. The maximum attractive force, which occurs at $r \cong (R - \sigma)$ is somewhat larger than it is in the shell model [Fig. 3(b)]. This is a consequence of "extra shells" of virtual boundary particles present in the mean field beyond the single shell considered in the Lennard-Jones and Devonshire model. The larger maximum in the spherical system relative to cubic system [Fig. 3(c) vs 3(d)] is due to the fact that the boundary is a curve in the former and a plane in the latter; that is, for the spherical case a particle inside the simulation region is exposed to a larger number of virtual particles outside the boundary within the cut-off radius, R_{cut}. A very important difference between the MFFA model and the simpler models is that the repulsion which sets in as the particle approaches the boundary is considerably "softer" in the former than in the latter. The reason for this is the adiabatic nature of the MFFA model. A particle in the reaction zone "sees" a density given by the average structure around that particle for interactions with the virtual particles outside the boundary. The boundary responds adiabatically to the approach of a particle and the closest distance between a particle and a virtual particle is equal to the value of r where $g(r)$ first becomes nonzero.

As a particle penetrates into the boundary region the simple adiabatic model breaks down since the adiabatic force must vanish as the particle leaves the simulation zone. Physically, the solvent density should no longer adjust adiabatically when the particle is near or outside the boundary; instead the force seen by the particle should become similar to the Einstein restoring force felt by it as it collides with its first solvation shell.[24] A simple extension of the MFFA force beyond the boundary is accomplished by numerically fitting a linear region of the force just inside the boundary [see Figs. 3(c) and 3(d)] so that the linearized boundary force remains repulsive. The slope chosen is the minimum value necessary for the density to remain equal to the mean density ρ_0 as the boundary is approached. This is accomplished by examining the density variation in short simulations employing possible sets of linear force parameters. Too soft a restoring force for

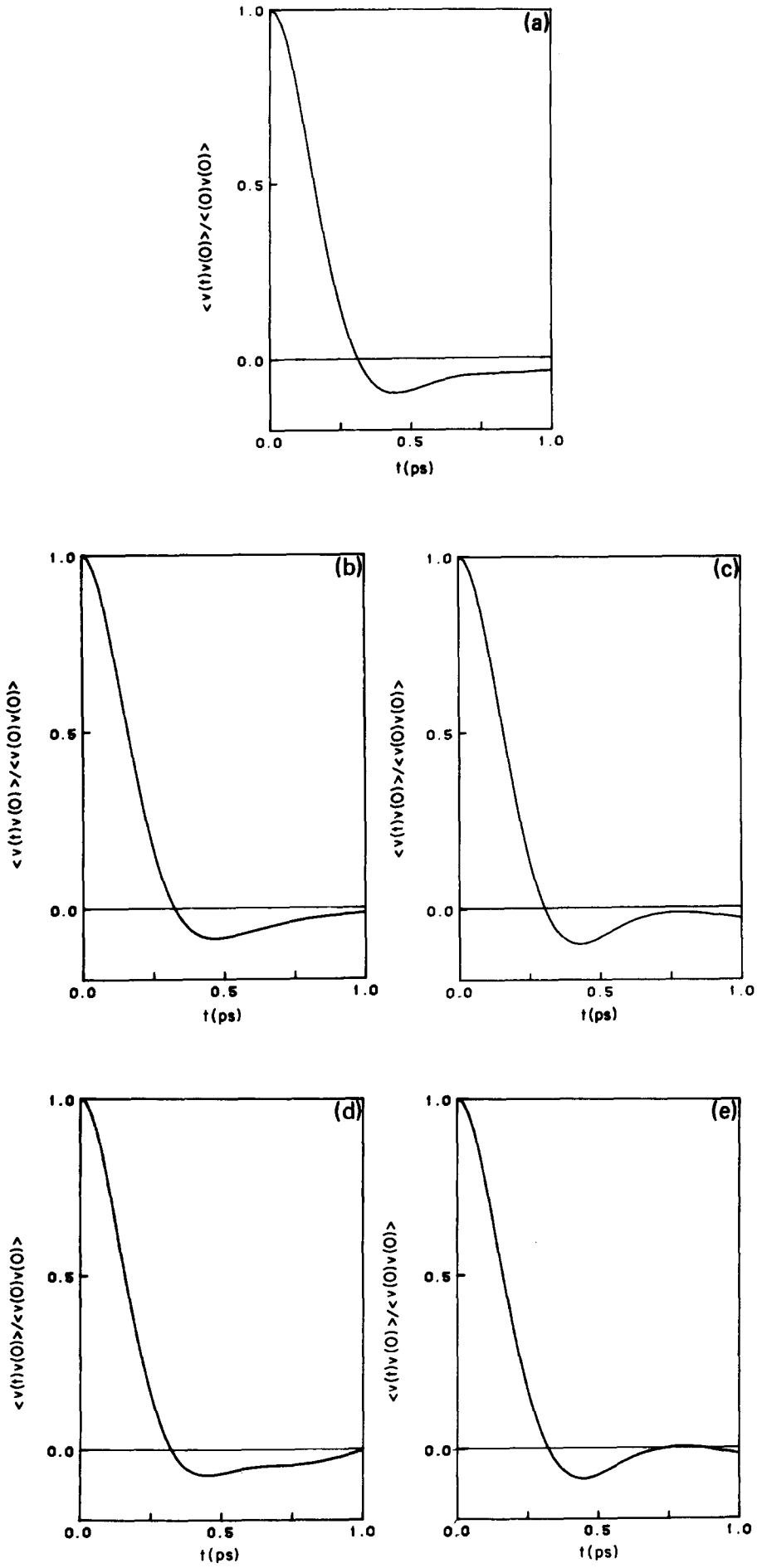

FIG. 4. Velocity autocorrelation functions. The normalized velocity autocorrelation function is plotted vs time (in ps) for: (a) conventional molecular dynamics simulation; (b) simulation with deformable boundaries at $z = \pm 9.67$ Å of a cube; (c) simulation with deformable stochastic boundaries on a cube. (The stochastic buffer region begins at $z = \pm 8.67$ Å); (d) simulation with deformable boundaries at the surface of a 12.0 Å sphere; (e) simulation with deformable stochastic boundaries on a 12.0 Å sphere. (The stochastic buffer region begins at $R = 11.0$ Å.)

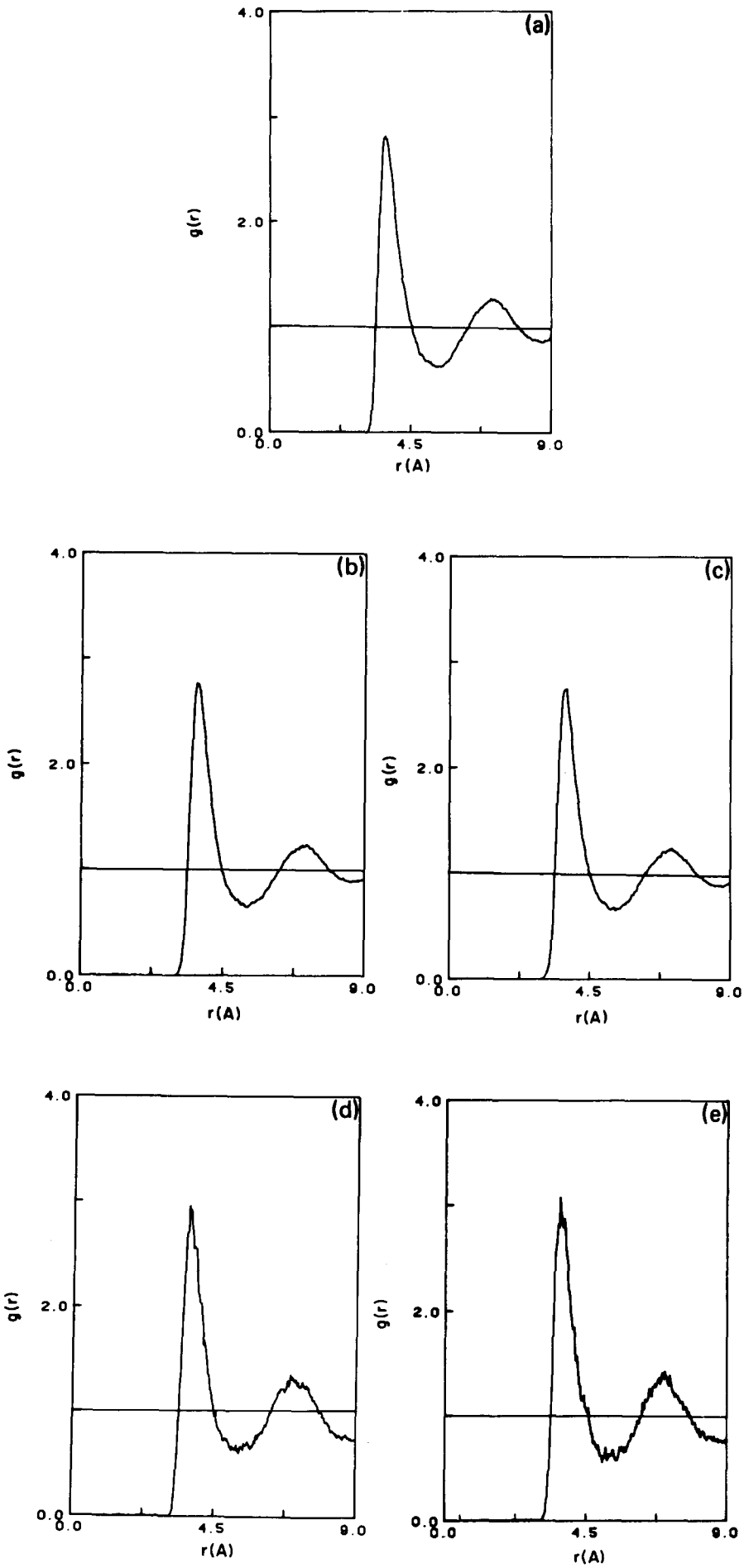

FIG. 5. Radial distribution functions. The radial distribution function is plotted versus radial separation in angstroms. The figure descriptions correspond to (a)–(e) in Fig. 4.

the boundary region leads to a net density decrease within the simulation zone; too large a linear restoring force has little effect on the density. Comparing Figs. 3(b) and 3(c) in the repulsive region near the boundary, it is clear that the linear force lies between the rigid wall given by the fixed Lennard-Jones and Devonshire boundary and the adiabatic MFFA limit.

B. Test of the deformable stochastic boundary method

We present first the procedure employed in the various molecular dynamics simulations and then give the results. The simulations are designed to examine the effectiveness of the deformable MFFA boundary approach in reducing the number of particles required to reproduce correct dynamical behavior near the center of the simulation zone. Lennard-Jones argon particles with the same conditions ($T = 97$ K, $\rho_0 = 0.020\,54$ Å^{-3}, $R_{cut} = 2.25\sigma$) as described for the boundary force calculations (Sec. IV A) were used.

As a standard for comparison, a simulation of 149 particles in a cubic box with sides 19.34 Å and periodic boundary conditions was performed by conventional molecular dynamics techniques.[21] Two simulations for the same cubic box were carried out with deformable MFFA boundaries imposed at the box edges on the z axis. One simulation treated the entire simulation zone by molecular dynamics and the second included a stochastic buffer region between $z = \pm$ (8.67 to 9.67 Å). A corresponding pair of simulations using MFFA boundary conditions with and without a stochastic buffer region 1 Å thick was performed for 149 particles in a spherical box of radius 12 Å. To compare the results obtained with the MFFA boundary and periodic boundary conditions, the trajectories obtained from the five simulations were analyzed and several basic quantities were computed; they are the velocity autocorrelation function, the self-diffusion coefficient, the radial distribution function, and the local temperature and density. The results of simulations employing periodic boundaries and the deformable sto-

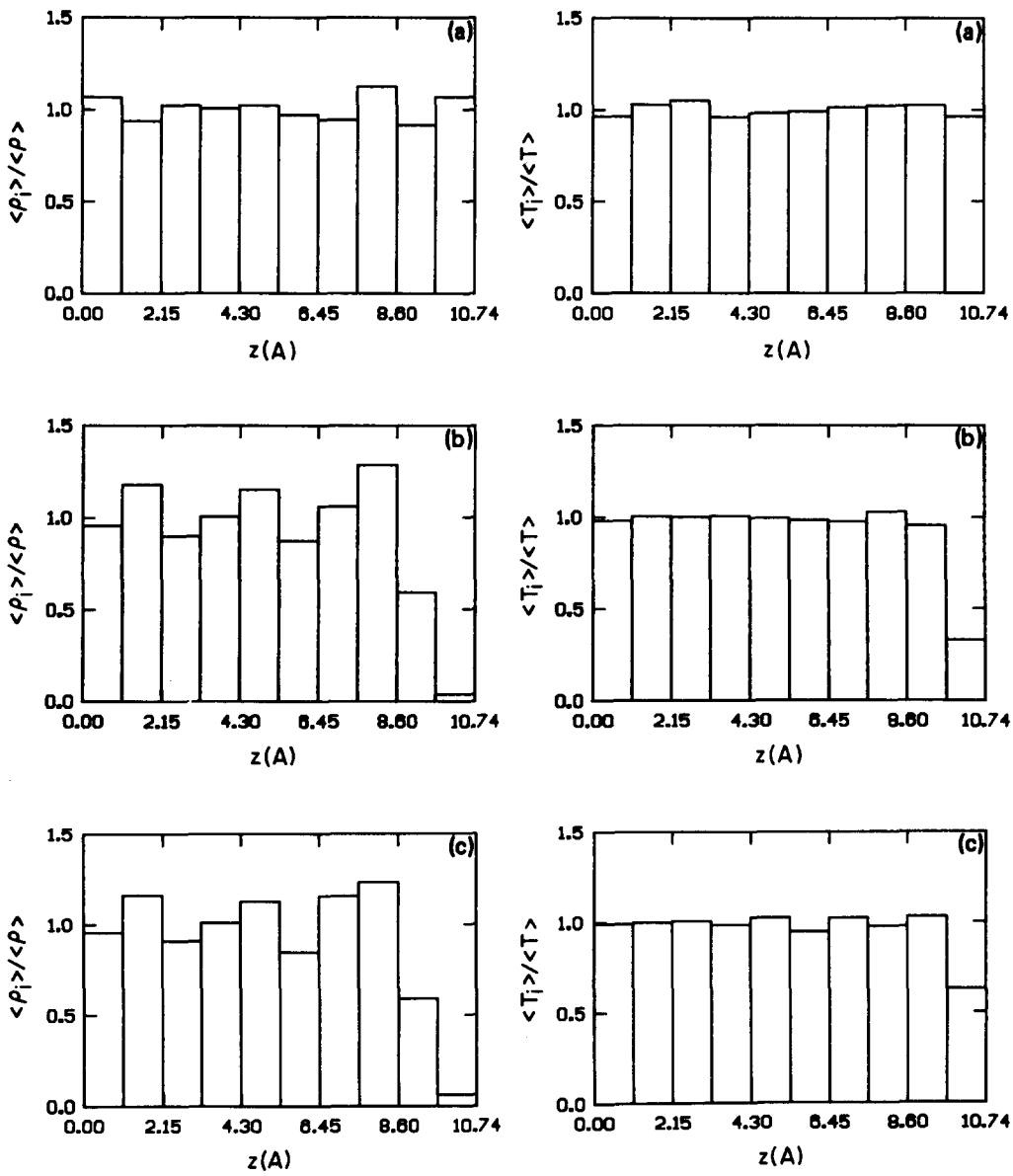

FIG. 6. Normalized local density and temperature profiles for the cubic simulation cases. The profiles are plotted vs distance from the origin along the z axis for: (a) the conventional molecular dynamics simulation case; (b) the deformable boundary case; (c) the deformable stochastic boundary case. The normalizing factors $\langle\rho\rangle$ and $\langle T\rangle$ appear in Table I.

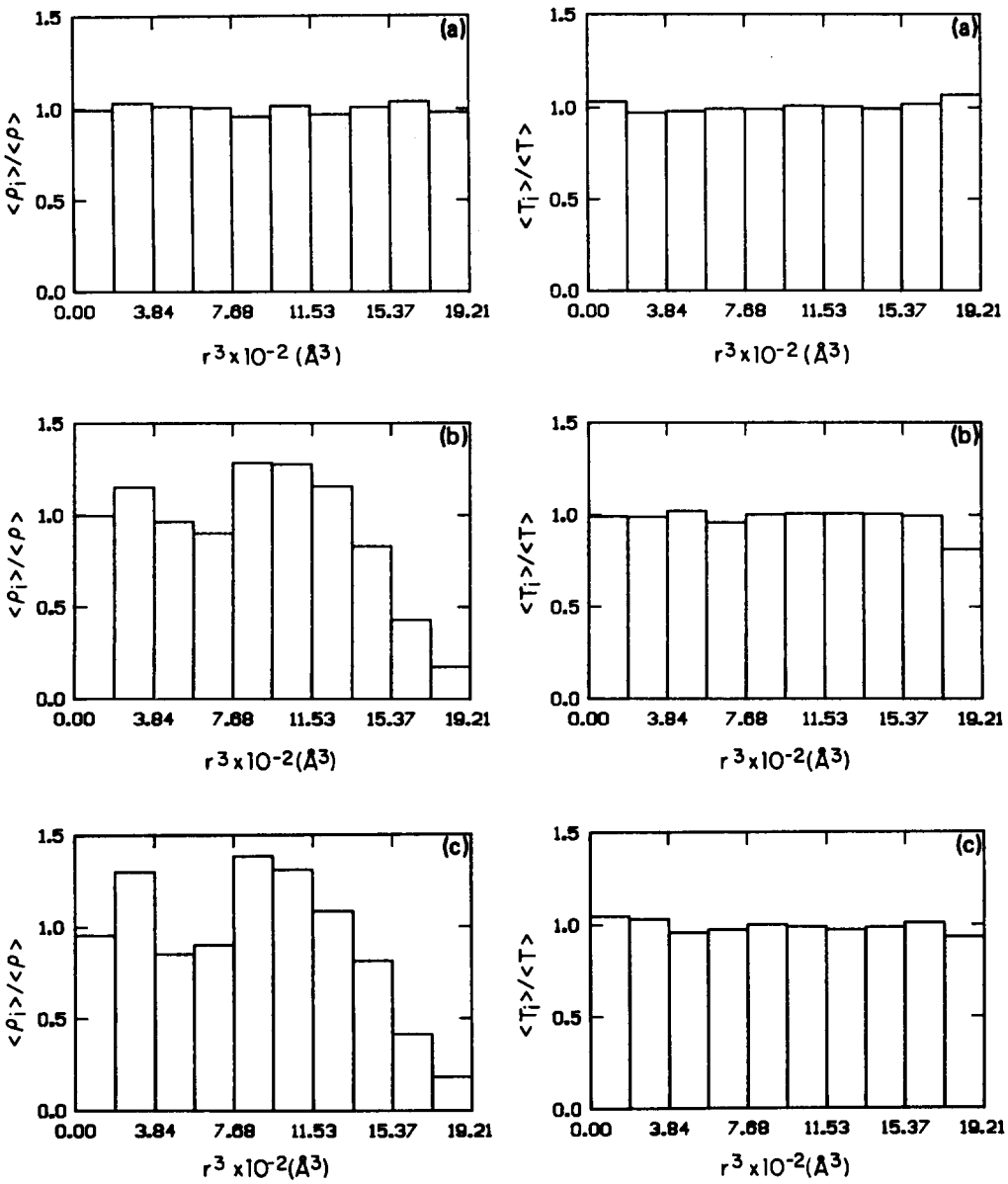

FIG. 7. Normalized local density and temperature profiles for the spherical simulation cases. The profiles plotted vs $r^3 \times 10^{-2}$ Å^3, are constructed from equal volume spherical shells. The figures represent results from: (a) the conventional molecular dynamics simulation (where the periodicity is used to construct spherical shells external to the cubic box); (b) the 12.0 Å radius (corresponding to $r^3 \times 10^{-2} = 17.28$ Å^3) spherical deformable boundary simulation; (c) the 12.0 Å radius spherical deformable stochastic boundary simulation.

chastic boundary approach are displayed in Figs. 4–7 and in Table II.

All of the molecular dynamics trajectories consist of 10–20 ps of equilibration followed by 18–20 ps of analysis. The integration scheme used is the Verlet algorithm with a time step of 0.01 ps; for the Langevin dynamics, the appropriately modified Verlet algorithm was employed.[25] The conventional molecular dynamics simulation started with the argon particles distributed on a simple cubic crystal lattice. The thermalization period consisted of about 5–10 ps of dynamics during which the velocities were chosen from a Boltzmann distribution every 0.5 ps to allow the system to evolve toward an equilibrium near the desired temperature; the thermalization was followed by 5–10 ps of equilibrium without velocity randomization. During the 18–20 ps of "production" dynamics which followed, the velocities and positions were stored on magnetic tape for subsequent analysis. The simulations not employing a stochastic buffer region used as a starting configuration the last production step from the conventional molecular dynamics. The appropriate boundary conditions were then imposed and the system was rethermalized. To introduce the stochastic buffer region, the additional terms given in Eq. (5) are added to the equations of motion for the particles in the buffer region; a configuration at the end of the appropriate MFFA boundary simulation was used and the system was rethermalized before the production dynamics.

1. Velocity autocorrelation function

The velocity autocorrelation function is a fundamental measure of the characteristic dynamics and is therefore considered the most sensitive test of the method. Since we are concerned primarily with representing solvent dynamics correctly within a "reaction" region we computed the velocity autocorrelation function for a subset of particles within a portion of the simulation box centered at the origin. For the simulations in which the boundaries are imposed on a cubic box only particles within the volume slab defined between $z = \pm 3.0$ Å were considered; for the simulations with a

TABLE I. Configurational sampling.

Simulation	Number of configurations[a]
Conventional molecular dynamics	149 000
Cube with deformable boundaries	50 000
Cube with deformable stochastic boundaries	49 000
Sphere with deformable boundaries	29 000
Sphere with deformable stochastic boundaries	25 400

[a] Number of atomic configurations sampled for all points along the radial distribution function and for the zero time value of the velocity autocorrelation function; for the latter, the number of configurations decreases approximately inversely with the time.

spherical simulation box only the particles inside a 6.0 Å sphere, centered at the origin, were included. In the analysis of the conventional molecular dynamics simulation the entire system was used.

Figure 4 shows the velocity autocorrelation functions for the standard molecular dynamics simulation [Fig. (4a)] and the four test cases [Fig. 4(b)–4(c)]. Figure 4(a) is in close agreement with the earlier results of Rahman.[21(a)] All of the test cases are in very good agreement with the conventional molecular dynamics results, particularly for the first 0.5 ps; that is, the curves cross zero at the correct time and have a minimum that is close to the exact result, although the longer time behavior is variable. The best long time behavior is obtained for the cubic box. This may be due in part to the fact that the cubic box with periodic boundary conditions in two directions is closer to the conventional simulation system. Also, the sampling error is smaller because a larger number of particle configurations are included in computing the velocity autocorrelation functions than in the other cases (see Table I). We note also that the overall behavior of the velocity autocorrelation function is slightly better for simulations not including a stochastic buffer region. This observation seems somewhat puzzling in light of the comment by Berkowitz and McCammon[13] that a stochastic buffer region was essential to ensure reasonable results. The discrepancy may be a consequence of the differences in the two reservoir region models; the wall force used here is softer than that employed by Berkowitz and McCammon.

Table II lists the values of the self-diffusion coefficients computed from the integral of the velocity autocorrelation function. A value is included for the self-diffusion obtained by Rahman.[21(a)] The 3% difference in the diffusion constant from the present standard simulation and that of Rahman is accounted for by the temperature difference,[26] although the agreement in the two values may be somewhat fortuitous since we have calculated D from the integral of the velocity correlation function and not the long-time slope of the mean square displacements. The computed values of the self-diffusion coefficient from the various boundary model simulations are all satisfactory. Agreement with the full dynamics improves somewhat as one goes from the spherical cases to the cubic cases.

2. Radial distribution function

The radial distribution function is computed in a manner similar to the velocity correlation function. For each dynamical configuration, the structure around the particles within the interior subvolumes (see the above) was determined and the equilibrium radial distribution function $g(r)$ representative of the average structure within the reaction region, was then computed. In the cubic cases, periodic images were included where they are appropriate (i.e., on the faces of the cube which are not represented by a deformable boundary).

The radial distribution functions are displayed in Fig. 5. All of the boundary force simulation results show generally very good quantitative agreement with the conventional molecular dynamics simulation in terms of peak heights and minima and their positions. There is more noise in the radial distribution function computed from the spherical simulation results due to the smaller volume included in the calculation. Also, the spherical simulation with the stochastic buffer region seems to have a higher, somewhat distorted second peak.

TABLE II. Summary of the simulation results.

Simulation	$\langle T \rangle$ (K)	$\langle \rho \rangle$ (Å^3)	D (cm^2/s)	T_{rms} (K)	ρ_{rms}
Conventional MD	97.0	0.020 54	2.50×10^{-5}	5.01	...
Cube with deformable boundaries	94.3	0.020 50	2.58×10^{-5}	4.24	0.000 12
Cube with deformable stochastic boundaries	94.1	0.020 46	2.57×10^{-5}	4.49	0.000 14
Sphere with deformable boundaries	96.4	0.020 11	2.66×10^{-5}	4.83	0.000 24
Sphere with deformable stochastic boundaries	96.8	0.020 02	2.93×10^{-5}	4.63	0.000 23
Rahman [Ref. 10(a)]	94.4	0.020 54	2.43×10^{-5}	1.56[a]	...

[a] The very small T_{rms} observed by Rahman is due to the large size of the system, 864 particles.

3. Local thermodynamic properties

To further test the boundary force results, local values of the mean temperature and density and their root-mean-square fluctuations were computed. The local quantities were obtained by dividing the simulation box up into regions of equal volume and computing the average value of the desired property within each region. The cubic box was divided into 18 equal volume regions along the z axis (the axis perpendicular to the deformable boundary), with symmetry equivalent volume regions on opposing sides of the midplane being averaged. This yielded nine equal volume slabs within the boundaries; one additional slab beyond the boundary was included to examine the extent of fluctuations outside the simulation box. For the spherical box, nine equal volume spherical shells were defined within the simulation boundary (i.e., between the origin and a radial distance of 12.0 Å); one equal-volume shell exterior to this region was included. The thermodyanamic properties were computed within each region over the entire simulation.

The local thermodynamic properties are displayed in Figs. 6 and 7. Figure 6 gives the local densities, $\langle \rho_i \rangle / \langle \rho \rangle$ and local temperatures, $\langle T_i \rangle / \langle T \rangle$ for the cubic box simulations and Fig. 7 gives those for the spherical box simulations; the subscript i denotes the average for region i and the unsubscripted quantity corresponds to the average over the entire simulation volume. Values of $\langle \rho \rangle$ and $\langle T \rangle$ and their fluctuations ($\rho_{\rm rms}$ and $T_{\rm rms}$, respectively), are listed in Table II for the various simulations.

The results in Fig. 6 for the cubic case with periodic boundaries show that the density and temperature are essentially homogeneous and there are no edge effects, as expected. For the boundary force models, the density for the various slabs has only a slightly greater variation [Figs. 6(b) and 6(c)] than for the conventional simulation [Fig. 6(a)]. We note that there is a small "edge effect" in the last two slabs inside 9.67 Å. The fact that there is very little density outside the simulation box (beyond $\pm$ 9.67 Å) indicates that the linear boundary force parameters were chosen optimally in this case. This is confirmed by the average density within the box, which is very near the input value (see Table II). The local temperatures are seen from Fig. 6 to show very little variation from the overall average temperature. This is in good agreement with the conventional dynamics results. The rms fluctuations in T are very similar in the three systems (see Table II).

For the spherical volume results obtained from the periodic boundary simulation, the local density and temperature shows only small variations (see Fig. 7). In the boundary models the local density has a significant variation between the equal volume shells [Figs. 7(b) and 7(c)] that is greater than that in the cubic cases [Figs. 6(b) and 6(c)]. Further, the "edge effect" is of more importance here, although it is somewhat overemphasized in the figure; i.e., the drop in density beginning at $r^3 = 1300$ Å corresponds to $r = 11$ Å in the 12 Å radius sphere. The density outside of the 12.0 Å sphere ($r^3 > 1728$ Å^3) is larger than in the cubic cases. This may arise from a less than optimal linear fit to the boundary force. The localized temperatures, $\langle T_i \rangle$, shows excellent agreement with the conventional molecular dynamics simulation. The rms fluctuations in the temperature are very similar in the three systems; the density fluctuations for the spherical boundary are about twice those for the cubic boundary simulations.

V. CONCLUDING DISCUSSION

A deformable stochastic boundary approach has been introduced for eliminating nonparticipating solvent particles from the simulations of the dynamics of localized processes. In this way a small volume system can be studied without the need for periodic boundary conditions. The structural, dynamic and thermodynamic properties calculated for spherical and cubic systems with such boundaries are in satisfactory agreement with the results of conventional molecular dynamics simulations.

The deformable stochastic boundary condition approach, as well as other special techniques (e.g., activated dynamics) are of interest for many cases that cannot be treated effectively by standard methods. Often it is necessary to reduce the size of the system so as to decrease the computational requirements; this can now be done by omitting distant solvent molecules in simulations of localized processes. Also, systems with thermal gradients, such as are generated by exothermic processes, can be treated by the present method which avoids unphysical heating effects that arise in conventional periodic boundary methods.[5]

While the present paper is confined to treating boundary effects in the dynamics of atomic solvent surrounding a stationary reactive site, the concepts introduced can be and are being applied to more general situations. Simulations of molecular, rather than atomic, solvents are possible by use of the mean field force approach.[27] In addition, the ideas embodied in the mean field approach may be useful in Monte Carlo studies of nonperiodic systems. Also, a generalized Langevin approach is being developed which eliminates distant, nonparticipating, regions of large molecules. This approach, when combined with the present methodology, will greatly reduce the computational effort associated with the simulation of the reaction dynamics of biomolecules (e.g., proteins and nucleic acids) in solution.[28] Furthermore, extension of the present approach to treat the dynamics of a "diffusing" reaction region may be useful. The methodology required for this case will include some of the ideas introduced in simulations of the dynamics of a diffusing reaction system on a host solid surface.[29]

We expect to employ the methodologies described here for the study of the dynamics of processes in macromolecules of biological interest. A particular concern is with enzymatic reactions, which involve long time scales and often take place at an interface between the protein and surrounding solvent. Further, the present approach may permit one to study important motional properties such as they decay of fluorescence anisotropy[30] and NMR relaxation[31] in macromolecules on the nanosecond time scales of present day experiment.

APPENDIX

In this section, we review the Lennard-Jones and Devonshire cell model[19] boundary force used by Stace and

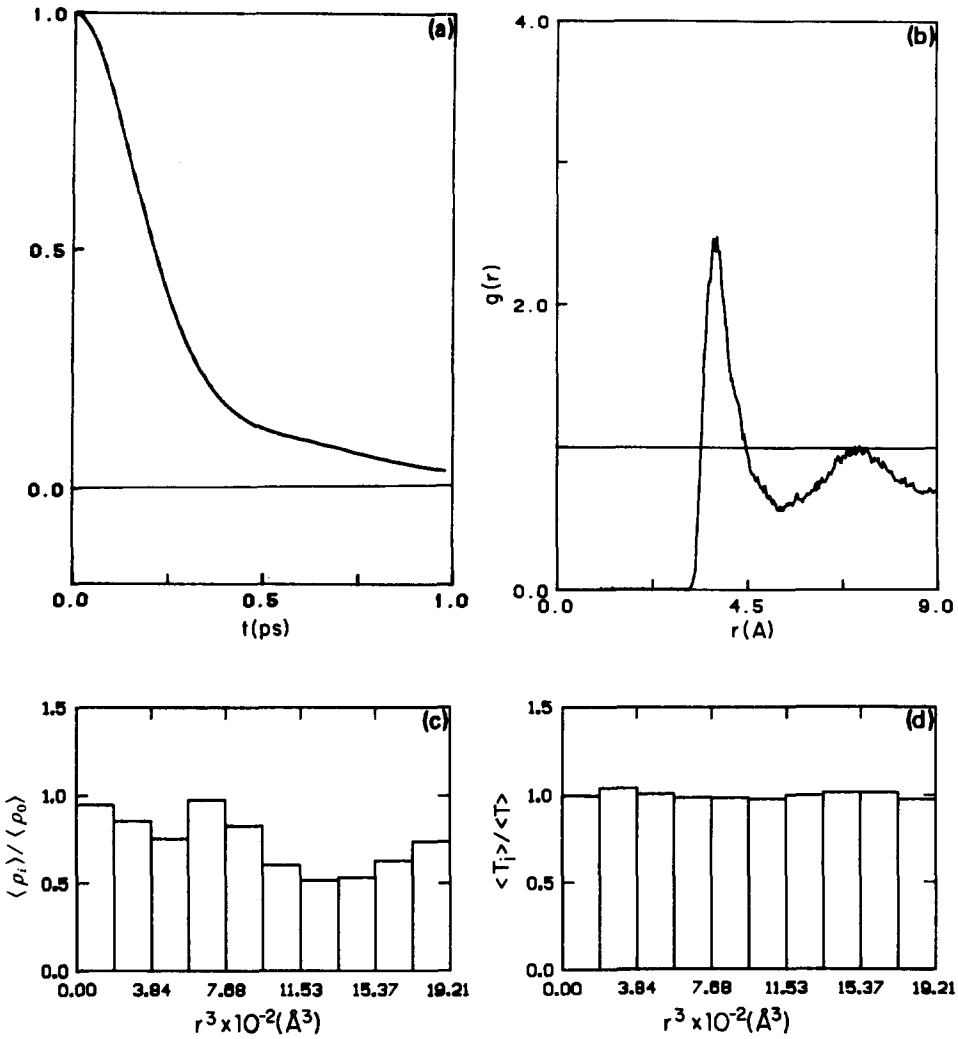

FIG. 8. Results from the cell model boundary force simulation. (a) The normalized velocity autocorrelation function versus time. (b) The radial distribution function vs radial separation. (c) The normalized density and temperature profiles vs $r^3 \times 10^{-2}$ Å^3. Note that the density profile is normalized to ρ_0.

Murrell[3] in the simulation of atomic recombination reactions in an inert gas solvent and determine the effect of this force on the properties of particles within the simulation zone. The wall or boundary force can be expressed as a function of the distance of an atom from the center of the simulation box (in our analysis it is assumed to be spherical) by use of arguments paralleling those of Stace and Murrell.[3] (i) The number density of atoms in the box is fixed at the value ρ_0. Thus, for a given radius, R, of the spherical box there are $N = \rho_0 4\pi R^3/3$ particles within the volume $4\pi R^3/3$. (ii) If the radius of the atoms is $\sigma/2$, the number of atoms lying in the spherical shell between $R - \sigma/2$ and $R + \sigma/2$ is

$$N_S \approx 4\pi\rho_0 R^2 \sigma \quad (\text{if } \sigma \ll R), \tag{A1}$$

assuming a uniform distribution of particles within the volume. This number, N_S, is the number of particles making up the rigid wall at R. (iii) The interaction potential between the wall (i.e., the N_S particles which are fixed rigidly and uniformally on the surface at R) and one of the N_I particles in the simulation region ($N_I = N - N_S$) is calculated by integrating the Lennard-Jones potential over the surface at R and multiplying by the number of particles per unit surface area, $N_S/4\pi R^2$; that is,

$$V(r_0) - V(0) = N_S \sigma^6 \epsilon/2 \times \left\{ \left[\frac{\sigma^6}{5Rr_0} \left(\frac{1}{(R - r_0)^{10}} - \frac{1}{(R + r_0)^{10}} \right) - \frac{4\sigma^6}{R^{12}} \right] + \left[\frac{1}{2Rr_0} \left(\frac{1}{(R + r_0)^4} - \frac{1}{(R - r_0)^4} \right) + \frac{4}{R^6} \right] \right\}, \tag{A2}$$

where $V(0)$ is the potential at the center of the box; this is Eq. (A1) of Stace and Murrell.[3] The force on a particle in the simulation region at point $\mathbf{r}_0$ is given by

$$-\nabla_{r_0}[V(r_0) - V(0)];$$

it is purely radial in nature. It is this force for the case ($R = 12.0$ Å; $\rho_0 = 0.020\,54$ Å^{-3}) that is plotted in Fig. 3(b).

To investigate how the boundary force used by Stace and Murrell is manifested in the properties of particles within the reaction zone we have performed a molecular dynamics simulation of 149 argon like particles. This number of particles in the simulation zone is not consistent with the Stace-Murrell boundary conditions for a 12.0 Å simulation box at an overall density of 0.020 54 Å^3. Thus, we have computed the size of the simulation box from the following considerations: (i) The number of particles lying on the surface of the sphere (N_S) is given by Eq. (A1); (ii) the total number of particles (N) is related to the density and the radius of the

simulation box (see the above); (iii) the difference between these two numbers must be equal to the number of interior particles (N_I), so that

$$N_I = 149 = 4\pi\rho_0(R^3/3 - R^2\sigma). \quad \text{(A3)}$$

This equation was solved for the parameters $\rho_0 = 0.0205\,54$ Å^{-3} and $\sigma = 3.4$ Å to yield $N_S = 240$ and $R = 16.53$ Å.

The molecular dynamics simulation was carried out under the conditions described above for 40 ps with 20 ps of thermalization (reequilibration) and 20 ps of production. The simulation was started using as initial coordinates the last step from the deformable spherical boundary simulation. The average density within a 12.0 Å subvolume of the 16.53 Å radius simulation box was found to be $\langle\rho\rangle = 0.015\,13$ Å^3 with $\rho_{\rm rms} = 0.000\,48$ Å^3. The temperature and rms deviation in the temperature is $\langle T\rangle = 93.8$ and $T_{\rm rms} = 5.92$ K, respectively. The results from the analysis of this simulation are presented in Fig. 8. In Fig. 8(a) the velocity autocorrelation function for particles within a 6.0 Å spherical volume, centered at the origin, is plotted. It is apparent from this figure and also from the radial distribution function plotted in Fig. 8(b) that the dynamics and structure within this region are vastly different from what is expected for a fluid at ρ_0 and $\langle T\rangle$ [see, e.g., Figs. 4(a) and 5(a)]. The question arises as to whether one can vary R so as to obtain the desired velocity autocorrelation function and radial distribution function. Figure 8(c) shows the localized density profile normalized to ρ_0 (i.e., $\langle\rho_i\rangle/\rho_0$). The local density in the regions nearest the origin appear to be close to the desired value, ρ_0, while the form of the velocity correlation function and the radial distribution function are clearly dominated by the lower density regions further from the origin. Making R smaller while keeping N_I constant is not likely to solve this problem, since although $\langle\rho\rangle$ will increase the shape of the density profile will not be improved. Although this boundary model may be sufficient for some problems involving dilute and possibly even dense gases, it apparently does not provide a reliable means for simulating liquids in finite regions.

[1]W. W. Wood and J. J. Erpenbeck, Annu. Rev. Phys. Chem. **27**, 319 (1976); J. P. Hansen and I. R. McDonald, *Theory of Simple Liquids* (Academic, New York, 1976).
[2]For a brief review, see, D. Chandler, Acc. Chem. Res. **7**, 246 (1974); a more recent review is, S. A. Adelman, Adv. Phys. Chem. **53**, 61 (1983).
[3]A. J. Stace and J. N. Murrell, Mol. Phys. **33**, 1 (1977).
[4]D. L. Bunker and B. S. Jacobson, J. Am. Chem. Soc. **94**, 1843 (1972).
[5]P. Bado, P. H. Berens, and K. R. Wilson, Proc. Soc. Photo–Opt. Instrum. Engin. **322**, 230 (1982).
[6]M. Karplus and J. A. McCammon, Annu. Rev. Biochem. **53**, 263 (1983).
[7]See, for example, *Statistical Mechanics: Part A Equilibrium Techniques*, edited by B. J. Berne (Plenum, New York, 1977).
[8]L. R. Pratt and S. W. Haan, J. Chem. Phys. **74**, 1864, 1873 (1981).
[9]M. Rao and D. Levesque, J. Chem. Phys. **65**, 3233 (1976); F. F. Abraham, D. E. Schreiber, and J. A. Barker, *ibid.* **62**, 1958 (1975).
[10]W. C. Swope, H. C. Anderson, P. H. Berens, and K. R. Wilson, J. Chem. Phys. **76**, 637 (1982).
[11]S. H. Northrup, M. R. Pear, C. Y. Lee, J. A. McCammon, and M. Karplus, Proc. Natl. Acad. Sci. USA **79**, 4035 (1982).
[12]G. Ciccotti and A. Tenenbaum, J. Stat. Phys. **23**, 767 (1980); A. Tenenbaum, G. Ciccotti, and R. Gallico, Phys. Rev. A **25**, 2778 (1982).
[13]M. Berkowitz and J. A. McCammon, Chem. Phys. Lett. **90**, 215 (1982).
[14]J. C. Keck, Discuss. Faraday Soc. **33**, 133 (1962).
[15]J. B. Anderson, J. Chem. Phys. **58**, 4648 (1973).
[16]R. O. Rosenberg, B. J. Berne, and D. Chandler, Chem. Phys. Lett. **75**, 162 (1980).
[17]W. F. van Gunsteren, H. C. Berendsen, and J. A. C. Rullmann, Mol. Phys. **44**, 69 (1981).
[18]For a review, see, S. A. Adelman and C. L. Brooks III, J. Phys. Chem. **86**, 1511 (1982).
[19]J. E. Lennard-Jones and A. F. Devonshire, Proc. R. Soc. London Ser. A, **163**, 53 (1937).
[20]J. L. Lebowitz and H. Spohn, J. Stat. Phys. **19**, 633 (1978).
[21](a) A. Rahman, Phys. Rev. A, **136**, A 405 (1964); (b) D. Levesque and L. Verlet, Phys. Rev. A **2**, 2514 (1970).
[22]M. Abramowitz and I. A. Stegun, *Handbook of Mathematical Functions* (Dover, New York, 1972).
[23]The high accuracy IMSL routine DBLIN was employed to check the integration at various points.
[24](a)S. A. Adelman, J. Chem. Phys. **73**, 3154 (1980); (b) C. L. Brooks III and S. A. Adelman, J. Chem. Phys. **76**, 1007 (1982); (c) **77**, 484 (1982).
[25]The algorithm in the CLAMPS simulation package written by D. Ceperley at NRCC was used.
[26]Levesque and Verlet, in the extensive simulation study of argon reported in Ref. 21(b), were able to parametrize D as a function of density and temperature. For a constant density, they found D is proportional to T. Thus all differences in our simulation result for D and the result of Rahman [Ref. 21(a)] may be attributed to the differences in temperature.
[27]C. L. Brooks III and M. Karplus (to be published).
[28]W. F. van Gunsteren and M. Karplus, Biochem. **21**, 2259 (1982).
[29]J. C. Tully, J. Chem. Phys. **73**, 1975 (1980).
[30]J. R. Lakowicz and B. P. Maliwel, J. Biol. Chem. **258**, 4794 (1983).
[31]A. Riberio, R. King, C. Restivo, and O. Jardetzky, J. Am. Chem. Soc. **102**, 4040 (1980).